Impact of divalent ions on dynamics of pressure field in water films

Omar E. Godinez-Brizuela and Vahid Joekar-Niasar*

School of Chemical Engineering and Analytical Science, The University of Manchester, Manchester, United Kingdom, Oxford Road, M13 9PL

E-mail: vahid.niasar@manchester.ac.uk

Abstract

It is known that wettability is thermodynamically dependent on disjoining pressure in thin films, which is itself determined by the short-range and long-range surface forces. Disjoining pressure is referred to as the net pressure difference between the pressure in a thin film and the pressure in a bulk fluid. By changing the ionic strength and ionic composition, the electrostatic/electrokinetic forces change that result in the variation of disjoining pressure. This has been of particular interest in industrial applications such as low salinity waterflooding, which is an enhanced oil recovery technology. In this application, the electrolytes contains a mixture of ions. However, it is not known how the valency of ions influence the dynamics of disjoining pressure. In this work, we simulate the variation of ions composition and disjoining pressure in a thin film, induced by the reduction of the ionic strength in the bulk fluid. We simulate the initial equilibrium conditions under high ionic strength (high salinity) by solving the Poisson-Boltzmann equation. Then, the boundary ionic strength is reduced (low salinity) to initialise the transport of ions, which is simulated using the Poisson-Nernst-Planck equations. To investigate the impact of ionic composition on the ionic transport and consequently pressure change, all simulations have been done at the same low and high

ionic strength, but different ionic compositions, namely 1:1, 2:1 and 1:2 ions. Also, the impact of scaling between film thickness and Debye length on the disjoining pressure and contribution of electrokinetic forces versus the osmotic forces to the disjoining pressure are discussed.

Nomenclature

ϵ	Electric permittivity $[F/m]$
λ	Debye screening length $[m]$
ψ	Electrical potential $[V]$
ρ	Net charge density $[C/m^3]$
$\tilde{\phi}$	Dimensionless electrical potential
$\tilde{\Pi}$	Dimensionless osmotic pressure
$\tilde{\Pi}_{dyn}$	Dynamic osmotic pressure (dimensionless)
$\tilde{\Pi}_{eq}$	Equilibrium osmotic pressure (dimensionless)
$\tilde{\rho}$	Reduced charge density
$\tilde{c_i}$	Dimensionless concentration
$\tilde{P}$	Total dimensionless disjoining pressure
$\tilde{p}_{dyn}$	Dimensionless disjoining pressure relative to $\tilde{\Pi}_{dyn}$
$\tilde{p}_{eq}$	Dimensionless disjoining pressure relative to Π_{eq}
c_i	Concentration of i-th species $[mol/m^3]$
C_i^{∞}	Bulk concentration if i-th species $[mol/m^3]$
D_i	Diffusion coefficient of i-th species $[m^2/s]$
D_{ref}	Reference diffusion coefficient $[m^2/s]$
E	Electric field $[V/m]$
e_c	Electron charge $[C]$

I	Identity matrix
J_i	Total flux of i-th species
k_B	Boltzmann's constant $[J/K]$
N_A	Avogadro constant
n_x, n_y	Normal unit vectors in x and y direction.
P	Total pressure $[Pa]$
T	Absolute temperature $[T]$
t	Time $[s]$
U	Velocity $[m/s]$
z_i	Valency of i-th species

Introduction

Disjoining pressure is defined as the difference between the pressure in a thin film and the pressure outside the film (bulk fluid)[1] . Disjoining pressure is a direct result of the surface forces, including the short-range (structural, van der Waals) and long-range (electrokinetic, osmotic) forces, which are controlled by chemical interactions between the electrolyte and surface properties of the materials[2] . Given that water films can be formed in the order of 10nm or smaller[3–5] , the surface forces and most importantly electric field in the film are strong enough to influence the transport of ions and consequently the temporal variation of the disjoining pressure, which has rarely been investigated.

One of the key phenomena directly linked to the disjoining pressure in two fluid-phase systems is wettability, which shows the affinity of a fluid to a solid surface in presence of another immiscible fluid[6] . Wettability is an important parameter in two-phase flow, which

controls the fluid dynamics and fluid-fluid interface movements. Churaev and Sobolev[7] proposed a thermodynamic-based equation to relate the disjoining pressure to contact angle. This means that if the disjoining pressure is modified, there is a potential for change of wettability. In oil industry, wettability alteration by modification of ionic strength and ionic composition of water has been utilised in low salinity waterflooding, which is an enhanced oil recovery technology.[8–10] In this technology, water with lower ionic strength (compared to the initial water) is injected to replace the initial high-salinity water and to modify the wettability towards the more water-wet status.[9,11–14]

There is a general consensus that reduction of the ionic strength of the injected water, electrical double layer expands due to the increase of repulsive electrical forces.[9,15,16] This is further supported by the experimental observations that the occurrence of the effect is linked to presence of charged components in the oil and the surface charge of the substrate in the form of polar components and surface-charged substrates, such as clay.[9] The water film in which the variation of disjoining pressure takes place is composed of a complex array of clay particles in contact with water film and constrained by the oil-water interface. Figure 1 shows a sketch of the water film where the variation of electrokinetic and osmotic forces can happen due to the change of ionic solution in the bulk fluid. Given the current understanding of the relation between wettability, disjoining pressure, and solid-fluid chemical interactions, it is important to investigate the evolution of disjoining pressure due to the dilution of bulk fluid in low salinity waterflooding. This provides further understanding of a) the impact of valency of ions on magnitude of the disjoining pressure, b) time scale of the evolution of disjoining pressure for different ions pairs.

The classical understanding of this problem is commonly described using DLVO theory, which explains the equilibrium state of a thin film.[17] However, it fails to capture the dynamics of the problem. Under dynamic conditions, the disjoining pressure in the thin film is strongly influenced by electro-hydrodynamic effects, however modelling of electro-hydrodynamics has been historically challenging because it involves coupling multiple non-linear equations to

account for electrophoresis and electro-osmosis for multiple species simultaneously. This modelling effort often includes solving equations for transport of ions, the electric potential field, and momentum and charge conservation.[18]

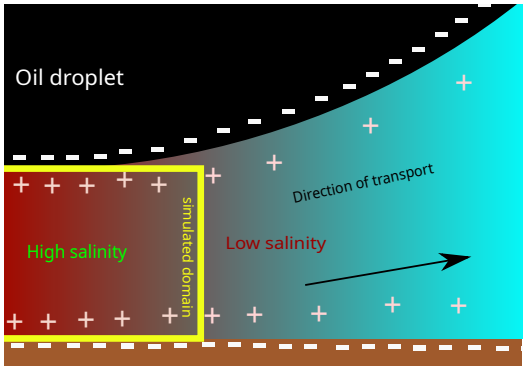

Figure 1: Sketch of a water film confined between oil and a substrate, which are both negatively charged (inspired from the droplet experiments of Mahani et al.[9]). The yellow box shows the schematic numerical domain.

Due to the importance of physical length scale for the magnitude of disjoining pressure, a multitude of research studies investigated the disjoining pressure at equilibrium conditions for different film thicknesses[4,5,7,19–24]as well as the deformation of fluid-fluid interfaces due to the disjoining pressure.[7,25–27] However, almost none of these studies provide insights into the dynamics of disjoining pressure and the impact of valency of ions on transport time scale and disjoining pressure in water films.

The ionic composition and ionic strength of brine in low salinity waterflooding has a critical role in wettability alteration and large-scale flow cell experiments have shown a distinct difference between the behaviors of monovalent and divalent ions.[28,29] It has been speculated that the divalent ions tend to become adsorbed on the charged surface, which is the basis of another hypothesis of low salinity waterflooding referred to as the multi-ion exchange mechanism.[15,30–32] The importance of divalent ions in microfluidic applications has been studied previously. Datta[33] et al developed a sorption model to account for the effect of Ca^{+2} and Mg^{+2} ions in electro-osmosis. Zheng et al.[34] found that the presence of

multivalent ions significantly reduces the effect of electro-osmosis because o the increased charged surface-ion interaction. However, regardless of the chemical interaction between the divalent ions and the solid surface, the role of divalent ions on dynamics of electrokinetic forces and disjoining pressure is not understood.

To model these electro-kinetic phenomena, it is often necessary to establish how the system behaves under equilibrium conditions. This is typically modeled using the Poisson-Boltzmann equation (1), which dictates the form of the electric potential under the assumption that the concentration profiles for the ions follow the Boltzmann distribution. This type of model has been widely used, although due to the non-linearity of the Poisson-Boltzmann equations, analytical solutions are only available for particular boundary value problems.[35]

$$\nabla^2\psi = -\frac{N_A e_c}{\epsilon}\sum_i z_i C_i^{\infty} exp(\frac{-z_i e_c \psi}{k_B T}) \tag{1}$$

where ψ represents the equilibrium electric potential, N_A, e_c, k_B, ϵ and T represent the Avogadro number, the elementary charge, the Boltzmann constant, the medium permittivity and the temperature, accordingly. The indexed quantities z_i and C_i^{∞} represent the charge and bulk concentration for the i-th ion species accordingly.

Under transient conditions, the Poisson-Nernst-Planck system of equations can be used, where the Nernst-Planck equations governs the transport of each ion, including the electrophoretic migration produced by the electric field. In this coupled system, the electric potential can be calculated using the Poisson Equation. This type of model has seen widespread use in the design of microfluidic devices, using numerical modelling.[36,37] The Poisson-Nernst-Planck model is described by equations 2a, 2b and 2c

$$\nabla^2\psi = -\rho/\epsilon \tag{2a}$$

$$\rho = N_A e_c \sum_i z_i c_i \tag{2b}$$

$$\frac{\partial c_i}{\partial t} = -\nabla\cdot(-D_i\nabla c_i + U c_i - \frac{z_i e_c}{k_B T} c_i \nabla\psi) \tag{2c}$$

where ρ is the net charge density, and c_i is the concentration of ion i, U is velocity and D_i is the binary diffusion coefficient for the ion i.

This work aims to expand the research carried out by Joekar-Niasar and Mahani.[38] In their original work, they modelled the evolution of the disjoining pressure in a film induced by the concentration drop at the boundary in the bulk fluid. Similarly we define the numerical domain such that it resembles the yellow box shown in Figure 1. Due to the numerical complexity of deformation of an interface while the force field is changing as well as the very short time scale of the problem shown here, we have considered a rigid domain in our simulations. Joekar-Niasar and Mahani[38] assumed the ions in the brine to be monovalent. However, in practical applications of low salinity waterflooding and the microfluidic experiments, divalent ions such as Ca^{+2} or Mg^{+2} are very common in practice and have shown to be more effective in change of contact angle. The asymmetric charge in the electrolyte may lead to different dynamics in the transport and re-stabilization of the pressure in the thin film and an increase magnitude of disjoining pressure and alternatively an improved wettability alteration. However, this has not been studied before and in this work we aim to delineate the impact of 1:1, 2:1 and 1:2 ion pairs on temporal change of disjoining pressure. We have set up the calculations such that the ionic strength remains the same for each ion pair.

Methodology

We aimed to model a liquid film trapped between the oil and the substrate, representative of the system previously described in literature[3,9,39] , which is schematized in Figure 1. We represented the film as a domain confined between two charged planes. Between these charged planes, an electrolyte composed of a series of different ions was modelled.

Initially, the system was set under equilibrium conditions for electric potential and ion concentrations, and then the boundary conditions for concentration at the edge of the do-

main was altered to simulate a change in salinity at the far field away from the film caused by the introduction of low salinity brine.

The computational domain we used to model this was a rectangle of aspect ratio 5:1. In our model the width of the domain was scaled accordingly based on their approximate Debye screening length as defined in equation (3)

$$\lambda = \sqrt{\frac{\epsilon k_B T}{e_c^2 N_A \sum_i z_i^2 C_i^\infty}} \tag{3}$$

where λ is the Debye length. The Debye length provides an approximation of the extent of the electrical double layer, which provides us with a benchmark to assess the effect of the overlapping of the electrical double layers of the parallel planes.

As initial conditions, the ion distribution profiles and electric potential were set to equilibrium as described by the Poisson-Boltzmann equation. Then, the ionic strength, $I = \frac{1}{2}\sum_i z_i^2 C_i^\infty$ at one of the boundaries of the domain was dropped to a tenth of its original value. We simulated the process through which the system acquires a new equilibrium concentration profile and observe the variation of the disjoining pressure throughout this re-stabilization process by testing multiple ion pairs including divalent ions, and film thicknesses.

Governing Equations

The governing equations are different for the two stages of the computation.

- The initial equilibrium conditions were found with a Poisson-Boltzmann model, which describes the electric potential under equilibrium conditions[18]

- The transient conditions were computed using a Poisson-Nernst-Planck system[40] coupling the Nernst-Planck equation for ion transport and the Poisson equation was used to update the electric potential field. Then, the a simplified momentum equation taking into account the body force created by the fluctuation in the electric field and

charge distribution was used to calculate the pressure field.

To obtain the initial conditions, the equilibrium electric potential is computed by solving the Poisson-Boltzmann equation (4).

$$\tilde{\nabla}^2\tilde{\phi} = -\frac{1}{\sum_i z_i^2 C_i^\infty}\sum_i z_i C_i^\infty exp(-z_i\tilde{\phi}) \tag{4}$$

where $\tilde{\phi}$ is the dimensionless electric potential $\phi = \frac{e_c\phi}{k_B T}$, and the nabla operator is made dimensionless following the relation $\tilde{\nabla} = \lambda\nabla$.

The equilibrium ionic concentrations for each ion i, were computed using equation (5), following the Boltzmann distribution.

$$\tilde{c_i} = exp(-z_i\tilde{\phi}) \tag{5}$$

where $\tilde{c_i}$ is the dimensionless concentration of the i-th species, made dimensionless by taking its ratio to the bulk concentration at initial conditions, $\tilde{c_i} = c_i/C_i^\infty$.

After the equilibrium conditions were computed, the transient part of the simulation was implemented using the a Poisson-Nernst-Planck formulation.[40] The ion concentrations are updated by solving the Nernst-Planck equation for each ion.

$$\frac{\partial\tilde{c_i}}{\partial\tilde{t}} = \frac{D_i}{D_{ref}}(\tilde{\nabla}^2\tilde{c_i} + z_i\tilde{\nabla}\cdot(\tilde{c_i}\tilde{\nabla}\tilde{\phi})) \tag{6}$$

The dimensionless time used in this equation is defined as $\tilde{t} = \frac{tD_{ref}}{\lambda^2}$, where D_{ref} is a chosen, reference diffusion coefficient. Since for our application both ions are assumed to have the same diffusion coefficient, the ratio of D_i and D_{ref} is equal to unity.

The ion flux for the i-th species J_i is defined by the relation described in equation (7).

$$J_i = -\tilde{\nabla}\tilde{c_i} - z_i\tilde{c_i}\tilde{\nabla}\tilde{\phi} \tag{7}$$

The electric potential was then solved using the Poisson equation in the form of equation (8).

$$\tilde{\nabla}^2\tilde{\phi} = \frac{\sum_i z_i C_i^{\infty}\tilde{c}_i}{\sum_i z_i^2 C_i^{\infty}} \tag{8}$$

At each time-step, the pressure in the film was computed with equation (9), which accounts for momentum conservation in a rigid domain.

$$\tilde{\nabla}^2\tilde{P} = \tilde{\nabla}^2\tilde{\Pi} + \tilde{\nabla}\cdot\tilde{\rho}\tilde{\nabla}\tilde{\phi} \tag{9}$$

Here, the dimensionless pressure is represented by $\tilde{P}$ and $\tilde{\rho}$ is the reduced charge density, defined as $\tilde{\rho} = \sum_i z_i\tilde{c}_i C_i^{\infty}$.

The osmotic pressure $\tilde{\Pi}$ is computed using equation (10) and (11) for equilibrium and non-equilibrium conditions, accordingly. Equation (11) is an alternative formulation for osmotic pressure to extend the validity of the original formulation for osmotic pressure to non-equilibrium conditions.[41,42]

$$\tilde{\Pi}_{eq} = \sum_i z_i^2 C_i^{\infty}(\tilde{c}_i - 1) \tag{10}$$

$$\tilde{\Pi}_{dyn} = \sum_i C_i^{\infty}\tilde{c}_i(1 - exp(z_i\tilde{\phi})) \tag{11}$$

We assume the domain is rigid ($U = 0$), therefore the momentum equation can be written as a direct relation between the pressure in the system and the Maxwell stress tensor as follows.

$$\nabla P = \nabla\cdot T \tag{12}$$

Where the Maxwell stress tensor is defined as follows.[43]

$$T = \Pi I + \frac{1}{2}\epsilon|E|^2 I - \epsilon E\otimes E \tag{13}$$

where E is the electric field $E = -\nabla\psi$, I is the identity matrix.

Boundary Conditions

The modelled domain, is a 5:1 aspect ratio rectangle representing a thin film with four boundaries labelled A, B, C, and D, which mimic the conditions of the yellow box shown in Fig.1. The boundary conditions for each part of the domain are defined and shown in Figure 2. Boundary A represents a symmetry axis to represent the vertical centra axis of a film in a cylindrical shape that is confined beneath the oil droplet, shown in Figure 1. Boundary B represents the edge of the thin film that is exposed to the bulk of the fluid (i.e. outside the thin film), where the concentration is dropped to 1/10th of its original value during the transient part of the simulation. Boundaries C and D represent the interfaces with the neighbouring fluid (oil) and the rock to which, for sake of simplicity, the same negative charge has been assigned. The negative charge is assigned by imposing a negative gradient of potential of -20 dimensionless units normal to these planes confining the film.

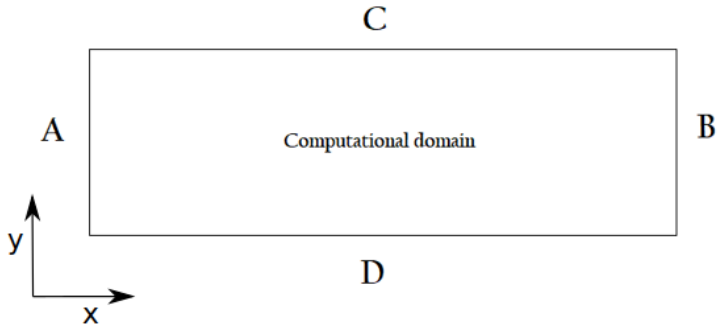

Figure 2: Schematic of the boundary conditions

for boundary A:

$$\tilde{\nabla}\tilde{c}_i \cdot n_x = 0; \qquad \tilde{\nabla}\tilde{\phi} \cdot n_x = 0; \qquad \tilde{\nabla}\tilde{p} \cdot n_x = 0;$$

for boundary B:

$$\tilde{c_i} = \begin{cases} C_i^{\infty}, & \text{for } t = 0 \\ 0.1C_i^{\infty}, & \text{for } t > 0 \end{cases}$$

$$\tilde{\phi} = 0; \qquad \tilde{p} = 0$$

for boundaries C and D:

$$J_i \cdot n_y = 0 \qquad \tilde{\nabla}\tilde{\phi} \cdot n_y = -20 \qquad \tilde{\nabla}\tilde{p} \cdot n_y = \tilde{\nabla}\tilde{\Pi} \cdot n_y + \tilde{\rho}\tilde{\nabla}\tilde{\phi} \cdot n_y$$

Where n_x, n_y represent unit vectors pointing in the x or y direction The concentrations at the bulk of the fluid during the initial conditions were selected such that two conditions was satisfied

- The bulk of the fluid was electrically neutral, and
- The ionic strengths of different solutions were the same, regardless of whether the ion pair was monovalent or divalent.

The boundary condition for the Poisson and Poisson-Boltzmann equation was a fixed potential gradient, such that it represents a system with constant charge at the boundaries.

Numerical solver

In order to carry out the calculation we have used OpenFOAM, a well-known finite volume library written in C++. OpenFOAM is typically used in generic computational fluid dynamics simulations,[44] and as such its built-in capabilities respond to those needs. It is however, possible to create new applications by allowing the user to define the equations to solve . For our application, we have developed a custom code that solved the previously defined governing equations. Each of the equations was solved sequentially for each time step.

To discretize the equations, we used the second order linear upwind scheme to discretize the divergence operators. The Laplacian operators were discretized using the second order central difference scheme. The time derivatives were discretized using the second order- backward Euler method. In order to solve the coefficient matrices, we used the preconditioned conjugate gradient method or the preconditioned bi-conjugate gradient method, depending on whether the matrix was symmetric or asymmetric. The preconditioners utilized were the DIC (diagonal-based incomplete Cholesky) or DILU (diagonal-based incomplete LU), accordingly.[45]

Second order central differences were used to discretize the Laplacian operators. The divergence operators were discretized using high resolution NVD/TVD (normalised variable and total variation diminishing) schemes and the time derivatives were treated using the backward Euler second order scheme. The computational domain was discretized using a structured square grid of 50 by 250 cells.

Our solver starts by solving the Poisson-Boltzmann equation to obtain the equilibrium electric potential under initial high ionic strength conditions. Then, we proceed to change the boundary concentration to 0.1 of the high ionic strength to trigger the transient simulation and transport of ions. The solver continues to solve Poisson-Nernst-Planck equations (instead of Poisson-Boltzmann) to update the ion concentration fields and electric potential. The solution of the Poisson-Nernst-Planck equations is repeated iteratively in an inner loop to guarantee the system is converged. After this, the new pressure field is obtained and then the solver proceeds to the next time step. This process is schematized in diagram as shown in Figure S.1.

Results

Validation of disjoining pressure calculation

To validate the computational model and the disjoining pressures, a set of test simulations were carried out with the objective of comparing the disjoining pressures obtained by the model to available experimental data. We have taken the experimental data provided by Karraker and Radke [46] and compared it to the disjoining pressures under equilibrium conditions produced by our model. In our simulations, we imitated the experimental conditions described by the original source as closely as possible. This comparison is shown in Figure 3.

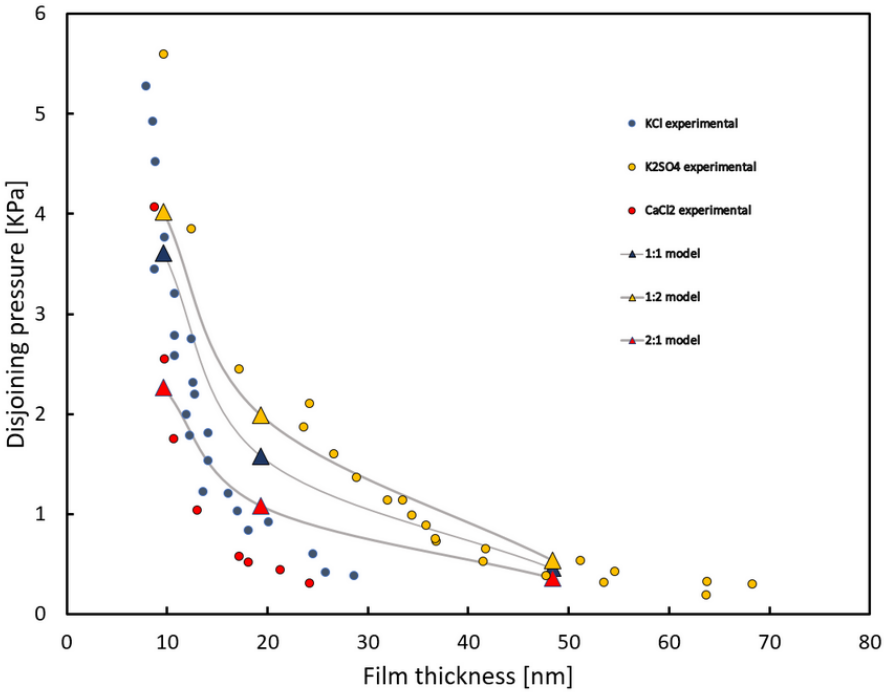

Figure 3: Average total disjoining pressures for a thin film P, compared to reproduced data from Karraker & Radke,[46] calculated with similar conditions of surface charge and bulk concentration as in the original source. The circles show experimental data while the triangles show the output of our model.

These disjoining pressures were measured in these experiments by equating it to the

capillary pressure in a thin film with different thicknesses. Even though the magnitudes of the disjoning pressures measured in the experiments and the ones produced by our model are not identical, they seem close to what is expected. Particularly, the span of the data seems to be a close match when comparing different ion pairs. The surface charge imposed in our model was equivalent to 0.002 C/m, which is within the range of values that were measured in the original experiments.[46] It must be noted that in the original experiments the surface charge was measured under different pH values, and under a number of other conditions that we cannot reproduce due to the limitations of our model and not every detail is available. The purpose of this comparison is merely to show that the model can roughly represent the pressures observed in real scenarios.This work was chosen for comparison primarily because it presents experimental measurements under uniform conditions for different ion pairs.

Transient ion concentration profiles

Calculations were carried out for two domain thicknesses of 0.2 (narrow) and 1.0 (wide) times the corresponding Debye length for each case, in order to see the effect of the increased overlapping in the electrical double layers. The calculations were done considering ion pairs with charges [+1,-1], [+2,-1], and lastly [+1,-2]. The bulk concentration of each case were chosen such that the ionic strength remained the same in all cases, regardless of the asymmetry of the ion charge.

After performing the simulations, the evolution of the average ion concentration is shown along the longitudinal direction in Figure 4 for all cases. In these , the initial and final states shown correspond to the values derived from the solutions to the Poisson-Boltzmann equation, for high and low ionic strength boundary conditions, accordingly. It is possible to see how the transient profile starts from the equilibrium position, and changes until it reaches the final state predicted by the values produced by the Poisson-Boltzmann equation. For the cases that include divalent ions, the difference in valence of the ions produces the asymmetric distribution profile observed in Figure 4 (c,d,e and f) , as compared to the

symmetric counterpart (a and b).

The electrostatic disjoining pressure profiles obtained are shown in Figure 5 and 6. The results included are shown for the values obtained using both formulations for osmotic pressure presented in equations (10) and (11), for equilibrium and non-equilibrium osmotic pressure, respectively. The results of the usage of the equilibrium formulation from Equation (8) is shown in Figure 5. In these results the initial and final states for the pressure are significantly different in this formulation, due to the net drop in disjoining pressure as a result of the net drop in concentration. This does not happen in the cases that include divalent ions, and the initial and final pressure are much closer to each other, which is also seen in the cases where the formulation for osmotic pressure was dynamic, shown in Figure 6. It is possible to notice immediately that in the divalent cation cases shown in Figure 5 (c) and (d) , show significantly different pressure field evolution trends when compared to (a), (b), (e) and (f). In the Figure 5 (c), the narrow domain shows a more abrupt change in pressure near the free boundary of the domain, whilst in (d), a large negative pressure change is observed. Sections (a) and (b) of Figure 5 show similar trends to (e) and (f), despite the latter including a divalent anion.

The pressure relative to the dynamic osmotic pressure formulation is shown in Figure 6. In here, similar results are observed. The initial and final states for the pressure profile are closer to each other, and the non-monotonicity trend observed before is also repeated here. In section (d) the large pressure drop shown in the equilibrium formulation is also observed in this case, and again, the cases that include a monovalent cation show similar results for their corresponding film thicknesses.

There is a clear pattern in the dynamics of the ion profile distribution. The positive ion seems to attain its final form much faster than the negative counterpart in all cases. It is during this delay period between the stabilization of the positive and negative ion concen-

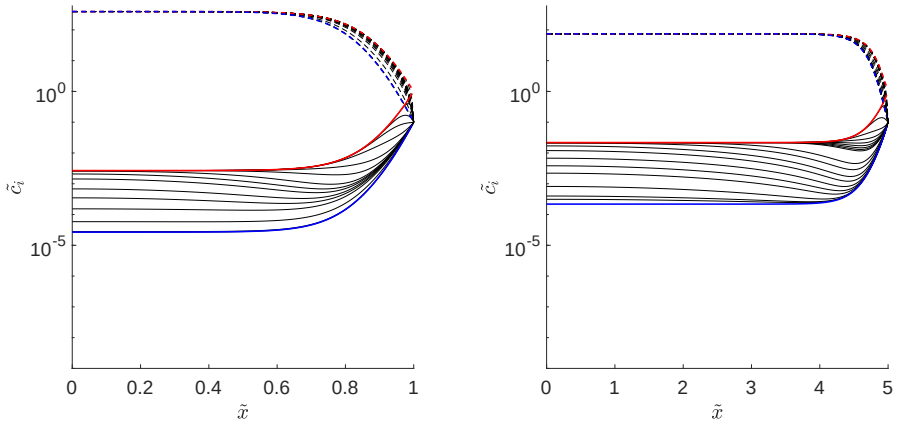

(a) Narrow , 1:1 ion

(b) Wide , 1:1 ion

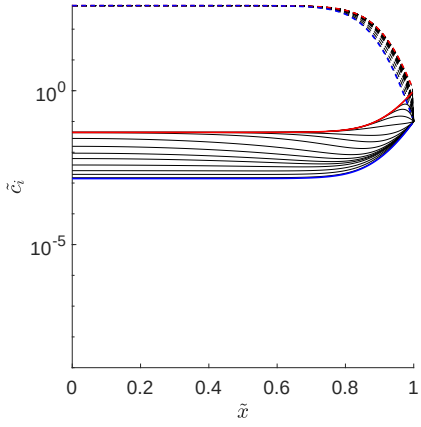

(c) Narrow , 2:1 ion

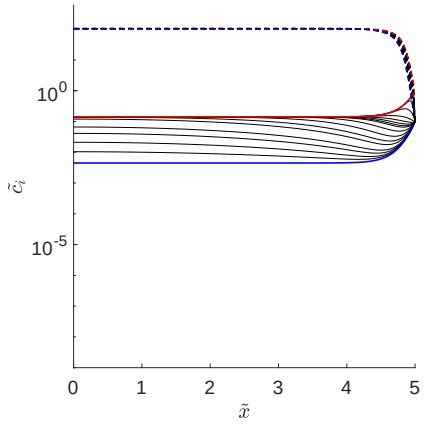

(d) Wide , 2:1 ion

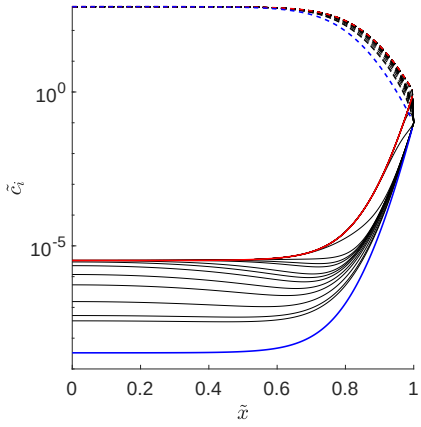

(e) Narrow , 1:2 ion

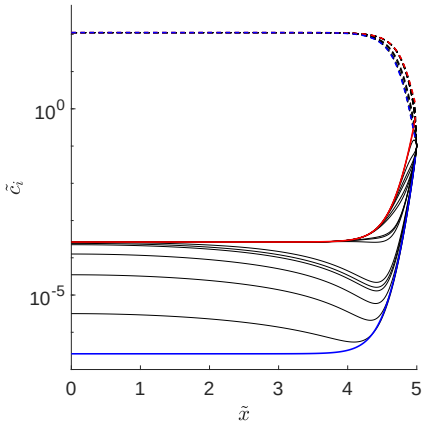

(f) Wide , 1:2 ion

Figure 4: Ion distribution profiles for the different configurations of film thickness and ion valences tested. The initial condition is shown in red and the final configuration is shown in blue, the positive ion is shown in dashed lines and the negative ion is shown in solid lines.

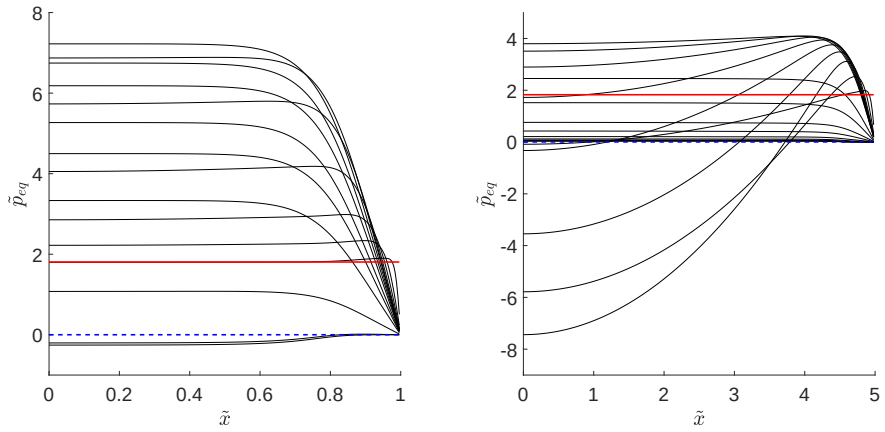

(a) Narrow , 1:1 ion

(b) Wide , 1:1 ion

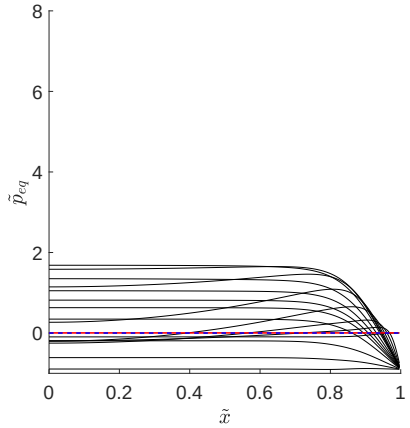

(c) Narrow , 2:1 ion

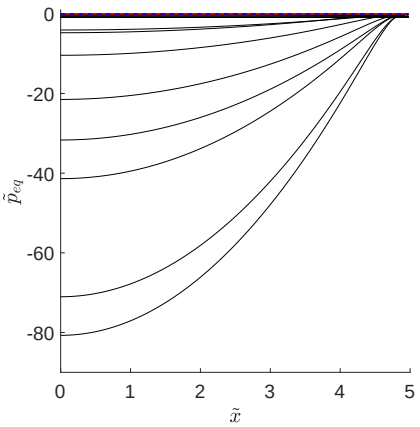

(d) Wide , 2:1 ion

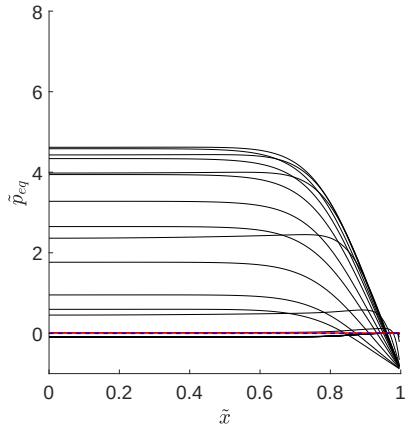

(e) Narrow , 1:2 ion

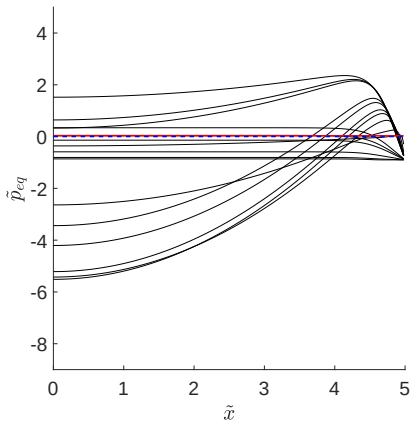

(f) Wide , 1:2 ion

Figure 5: Pressure profiles relative to the equilibrium formulation from equation 8. Shown for the different configurations of film thickness and ion valences tested. The initial condition is shown in red and the final configuration is shown in blue dashed lines. $\tilde{p}_{eq}$ represents the pressure field was computed relative to the equilibrium osmotic pressure, $\tilde{\Pi}_{eq}$ ($\tilde{p}_{eq} = \tilde{P} - \tilde{\Pi}_{eq}$).

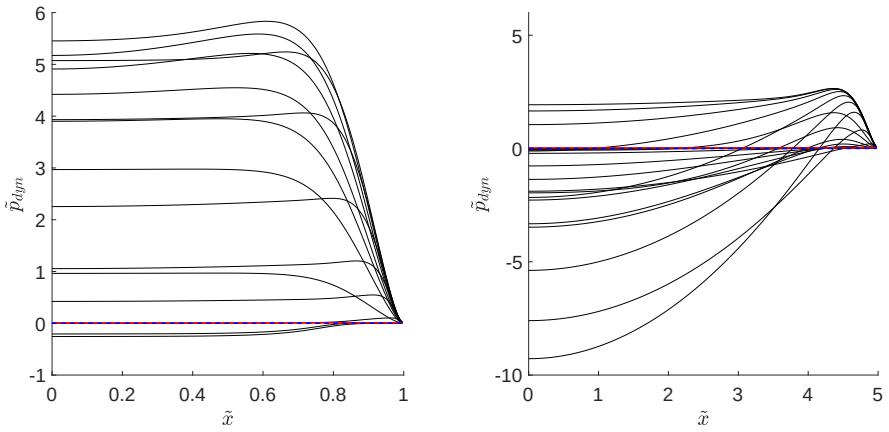

(a) Narrow , 1:1 ion

(b) Wide , 1:1 ion

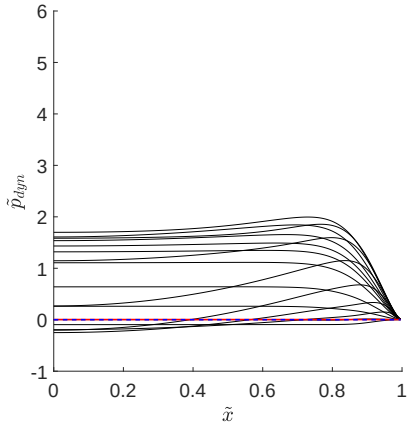

(c) Narrow , 2:1 ion

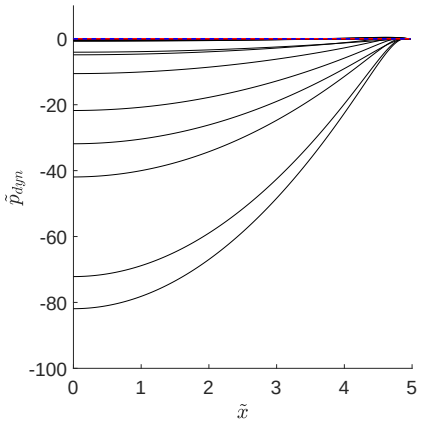

(d) Wide , 2:1 ion

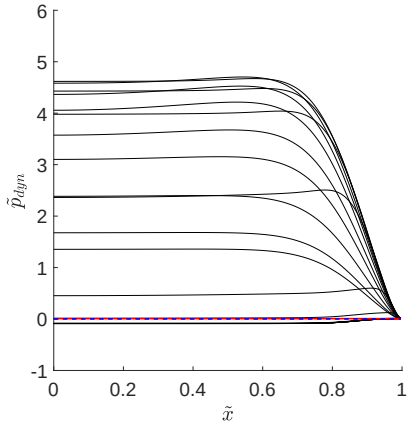

(e) Narrow , 1:2 ion

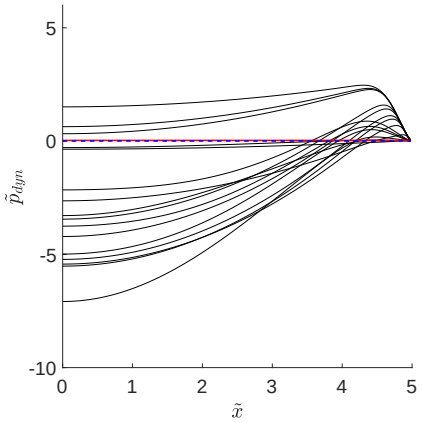

(f) Wide , 1:2 ion

Figure 6: Pressure profiles relative to the dynamic formulation from equation 9. Shown for the different configurations of film thickness and ion valences tested. The initial condition is shown in red and the final configuration is shown in blue dashed lines. $\tilde{p}_{dyn}$ represents the pressure field was computed relative to the equilibrium osmotic pressure, $\tilde{\Pi}_{dyn}$, ($\tilde{p}_{dyn} = \tilde{P} - \tilde{\Pi_{dyn}}$)

tration profiles that the non-monotonicity in the pressure field is observed. The pressure field is perturbed initially by the concentration drop, and the pressure in the system falls to the new equilibrium value as the concentration of the negative ion comes to its final configuration. This asymmetric behavior and the corresponding delay in the stabilization is only strengthened by the presence of divalent ions.

As Figure 4 shows the delay between the stabilization of the positive and negative ions occurs as the positive ion's initial and final concentration distributions are closer to each other compared to the ones with the negative ions. This is because the boundaries are negatively charged, and thus the positive ions are attracted to the charged walls, hence when the concentration profile is perturbed, they are already closer to their final state than the negative ions.

It can be seen that the divalent cation produces a lower pressure increase than the rest of the cases during the non-monotonic pressure variation. This can be related to an observation made in literature, specifying that monovalent cations are primarily responsible for changes in disjoining pressure,[47] since divalent cations tend to participate in sorption. With this we can speculate that the inclusion of divalent cations has a significance in the disjoining pressure even without the inclusion of sorption or steric effects mentioned in literature[30,31,48] and may have an influence of wettability alteration from the perspective of pure electrostatic forces. In the cases where the domain is wide, the pressure variation reaches negative values, particularly in the case of the case containing the divalent cations. This is because as the film becomes thicker, the electrostatic interactions become weaker, and the pressure becomes dominated by the osmotic component. Therefore, this suggests that the electrostatic interaction will yield a pressure increase only in a given range of film thicknesses, dependent on the present concentration of each ion, and their valency.

The presented results provide some insights into the role of electrostatic forces in low salinity waterflooding. Results imply that even without having ion exchange, the divalent cations lead to smaller repulsive disjoining pressure and less potential for low salinity effect.

Conclusions

An investigation on the effects on disjoining pressure caused by changes in ionic concentration was carried out. Monovalent and divalent ion pairs were tested under controlled ionic strength and constrained film thickness. Ion pairs containing divalent components exhibit a more abrupt change in concentration profile and an increased delay in the the re-stabilization of the system.

This has made apparent that the non-monotonicity of the total pressure in the thin film is linked to the delay in the re-stabilization of the ion pairs, since the positive ions attain their final configuration considerably faster than the negative ones.

This non-monotonicity in the film pressure is speculated to be tied to interfacial deformation, that may lead to variation of the contact angle observed in low salinity water flooding.

The pressure field evolution observed in ion pairs with monovalent cations seems to produce similar results, regardless of whether it is paired with a corresponding monovalent or divalent anion. By introducing the divalent cation, a much smaller variation in the disjoining pressure is observed compared to the systems that contain monovalent cations.

With this, we show that the forces acting on the thin film are sensitive to ion valency even without the inclusion of a sorption model, as the pressure profile attained with divalent cations is significantly different to the monovalent counterpart. Further investigation is needed to explore the role of film thickness under different ion valency conditions, and also it is necessary to establish the link between the deformation of the interface and the disjoining pressure produced by the electrostatic interactions.

Acknowledgement

The authors would like to thank the National Council of Science and Technology of Mexico (CONACyT) and the Energy Secretariat (SENER) for funding Mr. Godinez-Brizuela's PhD project, (Reference: 580914/461304).

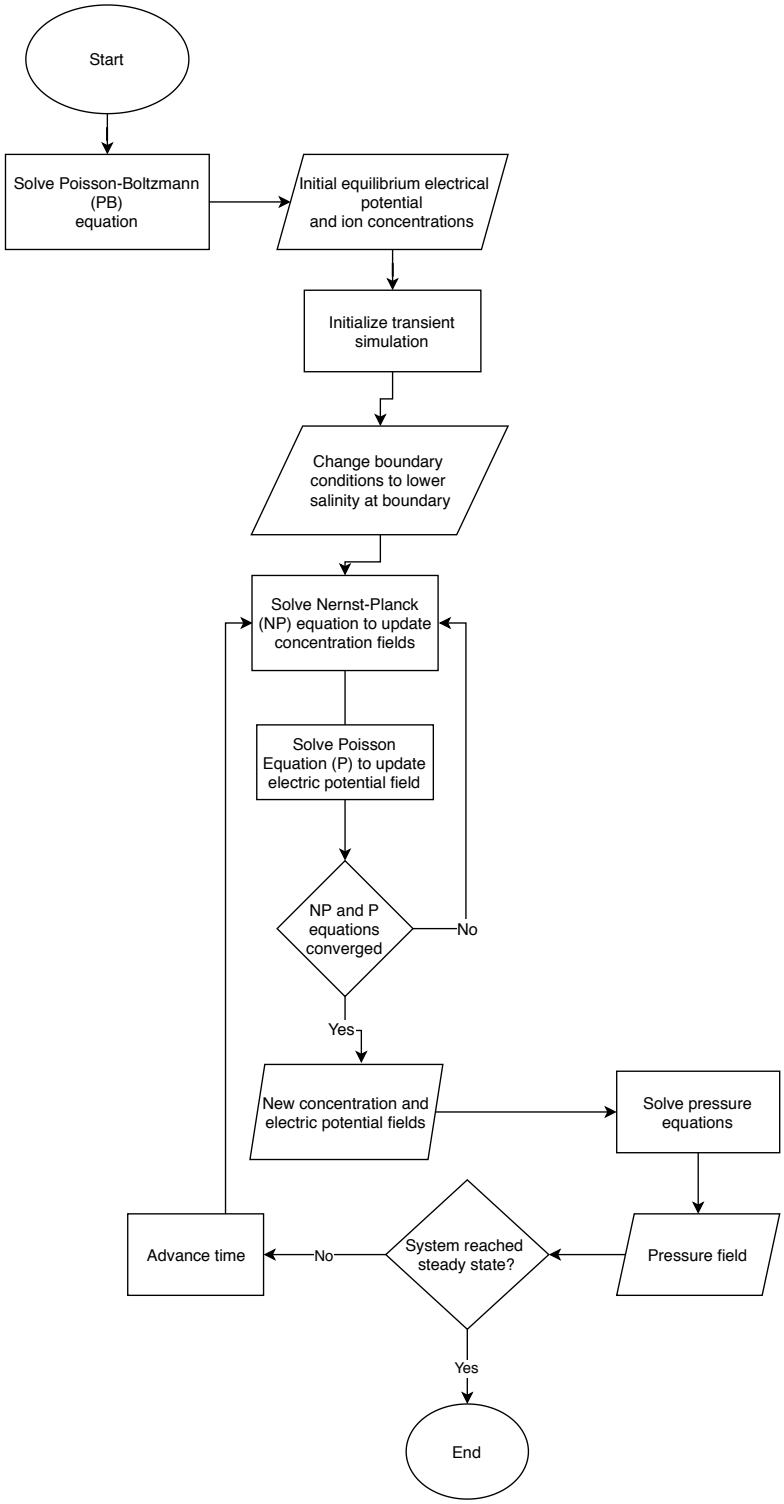

Figure S.1: Flow chart displaying the operation of the solver implemented.

References

(1) Adamson, A. W.; Gast, A. P. *Physical chemistry of surfaces*; John Wiley, New York, 1997.

(2) Dai, B.; Leal, L. G.; Redondo, A. Disjoining pressure for nonuniform thin films. *Physical Review E* **2008**, *78*, 061602.

(3) Bluteau, L.; Bourrel, M.; Passade-Boupat, N.; Talini, L.; Verneuil, E.; Lequeux, F. Water film squeezed between oil and solid: drainage towards stabilization by disjoining pressure. *Soft matter* **2017**, *13*, 1384–1395.

(4) Basu, S.; Sharma, M. M. Measurement of Critical Disjoining Pressure for Dewetting of Solid Surfaces. *Journal of Colloid and Interface Science* **1996**, *181*, 443455.

(5) Dimitrova, T. D.; Leal-Calderon, F.; Gurkov, T. D.; Campbell, B. Disjoining Pressure vs Thickness Isotherms of Thin Emulsion Films Stabilized by Proteins. *Langmuir* **2001**, *17*, 80698077.

(6) Kirby, B. J. *Micro-and nanoscale fluid mechanics: transport in microfluidic devices*; Cambridge university press, 2010.

(7) Churaev, N.; Sobolev, V. Prediction of contact angles on the basis of the Frumkin-Derjaguin approach. *Advances in Colloid and Interface Science* **1995**, *61*, 116.

(8) Hilner, E.; Andersson, M. P.; Hassenkam, T.; Matthiesen, J.; Salino, P.; Stipp, S. L. S. The effect of ionic strength on oil adhesion in sandstone–the search for the low salinity mechanism. *Scientific reports* **2015**, *5*, 9933.

(9) Mahani, H.; Berg, S.; Ilic, D.; Bartels, W.-B.; Joekar-Niasar, V. Kinetics of Low-Salinity-Flooding Effect. *SPE Journal* **2015**, *20*, 008020.

(10) Aziz, R.; Joekar-Niasar, V.; Martinez-Ferrer, P. Pore-scale insights into transport and mixing in steady-state two-phase flow in porous media. *International Journal of Multiphase Flow* **2018**, *109*, 51 – 62.

(11) Sheng, J. Critical review of low-salinity waterflooding. *Journal of Petroleum Science and Engineering* **2014**, *120*, 216224.

(12) Facanha, J. M. F.; Mahzari, P.; Sohrabi, M. Direct Observation of Low-Salinity Water Effect: Relationship Between Micro-Dispersion Formation and Wettability Alteration. *SPE Middle East Oil & Gas Show and Conference* **2017**,

(13) Ligthelm, D. J.; Gronsveld, J.; Hofman, J.; Brussee, N.; Marcelis, F.; Linde, H. V. D. Novel Waterflooding Strategy By Manipulation Of Injection Brine Composition. *EUROPEC/EAGE Conference and Exhibition* **2009**,

(14) Rivet, S.; Lake, L. W.; Pope, G. A. A Coreflood Investigation of Low-Salinity Enhanced Oil Recovery. *SPE Annual Technical Conference and Exhibition* **2010**,

(15) Myint, P. C.; Firoozabadi, A. Thin liquid films in improved oil recovery from low-salinity brine. *Current Opinion in Colloid & Interface Science* **2015**, *20*, 105114.

(16) Nasralla, R. A.; Nasr-El-Din, H. A. Double-Layer Expansion: Is It A Primary Mechanism of Improved Oil Recovery by Low-Salinity Waterflooding? *SPE Improved Oil Recovery Symposium* **2012**,

(17) Ohshima, H. *Electrical Phenomena at Interfaces and Biointerfaces*; John Wiley & Sons, Inc., 2012; pp 27–34.

(18) Masliyah, J. H.; Bhattacharjee, S. *Electrokinetic and colloid transport phenomena*; Wiley-Interscience, 2006.

(19) Li, D.; Neumann, A. Thermodynamics of contact angle phenomena in the presence of a thin liquid film. *Advances in Colloid and Interface Science* **1991**, *36*, 125–151.

(20) Choi, W.; Sharma, A.; Qian, S.; Lim, G.; Joo, S. W. Is free surface free in micro-scale electrokinetic flows? *Journal of Colloid and Interface Science* **2010**, *347*, 153155.

(21) Binks, B. P.; Cho, W.-G.; Fletcher, P. D. I. Disjoining Pressure Isotherms for OilWaterOil Emulsion Films. *Langmuir* **1997**, *13*, 71807185.

(22) Manica, R.; Connor, J. N.; Carnie, S. L.; Horn, R. G.; Chan, D. Y. C. Dynamics of Interactions Involving Deformable Drops: Hydrodynamic Dimpling under Attractive and Repulsive Electrical Double Layer Interactions. *Langmuir* **2007**, *23*, 626–637, PMID: 17209614.

(23) Onsager, L. The effects of shape on the interaction of colloidal particles. *Annals of the New York Academy of Sciences* **1949**, *51*, 627–659.

(24) Zhang, J.; Borg, M. K.; Reese, J. M. Multiscale simulation of dynamic wetting. *International Journal of Heat and Mass Transfer* **2017**, *115*, 886–896.

(25) Burrill, K.; Woods, D. Change in interface and film shapes for a deformable drop at a deformable liquid-liquid interface: Part I. Film hydrodynamic pressure distribution and interface shapes. *Journal of Colloid and Interface Science* **1969**, *30*, 511–524.

(26) Burrill, K.; Woods, D. Film shapes for deformable drops at liquid-liquid interfaces. II. The mechanisms of film drainage. *Journal of Colloid and Interface Science* **1973**, *42*, 15–34.

(27) De Feijter, J.; Rijnbout, J.; Vrij, A. Contact angles in thin liquid films. I. Thermodynamic description. *Journal of Colloid and Interface Science* **1978**, *64*, 258–268.

(28) Nicolini, J. V.; Ferraz, H. C.; Borges, C. P. Effect of seawater ionic composition modified by nanofiltration on enhanced oil recovery in Berea sandstone. *Fuel* **2017**, *203*, 222–232.

(29) Sohrabi, M.; Mahzari, P.; Farzaneh, S. A.; Mills, J. R.; Tsolis, P.; Ireland, S. Novel

insights into mechanisms of oil recovery by use of low-salinity-water injection. *SPE Journal* **2017**, *22*, 407–416.

(30) Omekeh, A. V.; Friis, H. A.; Fjelde, I.; Evje, S. Modeling of ion-exchange and solubility in low salinity water flooding. **2012**,

(31) Sorbie, K. S.; Collins, I. A proposed pore-scale mechanism for how low salinity water-flooding works. **2010**,

(32) Haagh, M. E. J.; Sîretanu, I.; Duits, M.; Mugele, F. Salinity-dependent contact angle alteration in oil/brine/silicate systems: the critical role of divalent cations. *Langmuir* **2017**, *33*, 3349–3357.

(33) Datta, S.; Conlisk, A.; Li, H.; Yoda, M. Effect of divalent ions on electroosmotic flow in microchannels. *Mechanics research communications* **2009**, *36*, 65–74.

(34) Zheng, Z.; Hansford, D. J.; Conlisk, A. T. Effect of multivalent ions on electroosmotic flow in micro-and nanochannels. *Electrophoresis* **2003**, *24*, 3006–3017.

(35) Chen, Z.; Singh, R. K. General Solution for PoissonBoltzmann Equation in Semiinfinite Planar Symmetry. *Journal of Colloid and Interface Science* **2002**, *245*, 301306.

(36) Mao, M.; Sherwood, J. D.; Ghosal, S. Electro-osmotic flow through a nanopore. *Journal of Fluid Mechanics* **2014**, *749*, 167183.

(37) Kler, P. A.; Lpez, E. J.; Dalcn, L. D.; Guarnieri, F. A.; Storti, M. A. High performance simulations of electrokinetic flow and transport in microfluidic chips. *Computer Methods in Applied Mechanics and Engineering* **2009**, *198*, 23602367.

(38) Joekar-Niasar, V.; Mahani, H. Nonmonotonic Pressure Field Induced by Ionic Diffusion in Charged Thin Films. *Industrial & Engineering Chemistry Research* **2016**, *55*, 62276235.

(39) Kumar, D.; Biswas, S. K. Contribution of different physical forces to the disjoining pressure of a thin water film being pressed by an oil droplet. *Journal of colloid and interface science* **2010**, *348*, 255–264.

(40) Krabbenhøft, K.; Krabbenhøft, J. Application of the Poisson–Nernst–Planck equations to the migration test. *Cement and Concrete Research* **2008**, *38*, 77–88.

(41) Butt, H. J.; Graf, K.; Kappl, M. Physics and chemistry of interfaces. 2003.

(42) Revil, A.; Linde, N. Chemico-electromechanical coupling in microporous media. *Journal of colloid and interface science* **2006**, *302*, 682–694.

(43) Stratton, J. A. *Electromagnetic theory*; John Wiley & Sons, 2007.

(44) Greenshields, C. The OpenFOAM Foundation. 2018; `http://www.openfoam.org/`.

(45) Behrens, T. OpenFOAM's basic solvers for linear systems of equations. 2009.

(46) Karraker, K.; Radke, C. Disjoining pressures, zeta potentials and surface tensions of aqueous non-ionic surfactant/electrolyte solutions: theory and comparison to experiment. *Advances in colloid and interface science* **2002**, *96*, 231–264.

(47) Ebeling, D.; van den Ende, D.; Mugele, F. Electrostatic interaction forces in aqueous salt solutions of variable concentration and valency. *Nanotechnology* **2011**, *22*, 305706.

(48) Bazant, M. Z.; Kilic, M. S.; Storey, B. D.; Ajdari, A. Nonlinear electrokinetics at large voltages. *New Journal of Physics* **2009**, *11*, 075016.